

Hydrodynamic Modeling of an Undulating Fin for Robotic Fish Design

Fangfang Liu, Can-Jun Yang, and Kok-Meng Lee, *Fellow, IEEE/ASME*

Abstract—Motivated by the interests to develop an agile, high-efficient robotic fish for underwater applications where safe environment for data-acquisition without disturbing the surrounding during exploration is of particular concern, this paper presents computational and experimental results of a biologically-inspired mechanical undulating-fin. The findings offer intuitive insights for optimizing the design of a fin-based robotic fish which has potentials to offer several advantages including low underwater acoustic noise, great maneuverability and better propulsion efficiency at low speeds. Specifically, this paper begins with the design of a robotic fish developed for experimental investigation and for validating computational hydrodynamic models of an undulating fin. A relatively complete computational model describing the hydrodynamics of an undulating fin is given. To analyze the effect of propagating wave motions on the forces acting on the fin surface, the three-dimensional unsteady fluid flow around the undulating fin is numerically solved using computational fluid dynamics (CFD) method. The pressure and velocity distributions acting on the undulating fin have been numerically simulated providing a basis to compute the forces acting on the undulating fin. The computational model has been experimentally validated by comparing the computed thrust coefficient against measured data based on a prototype flexible-fin mechanism.

Index Terms— robotic fish, biomimetic, undulating fin, computational fluid dynamics (CFD), hydrodynamic model, propulsion

I. INTRODUCTION

INTREST to inspect submerged structures (such as boats, oil and gas pipes), detect environmental pollution and deep sea exploration have motivated researchers and scientists to develop new concepts of underwater propulsion systems. Many different robotic devices are being developed to assess the benefits and study the ways of mechanisms utilized by fish and other aquatic animals to artificial systems [1-4]. Wave-like propulsion with wave propagating opposite to the swim direction has been found to be experimentally feasible [5]. The principle of employing flexural waves as a source of

Manuscript received February 1, 2010. This work was supported in part by National Natural Science Foundation of China (No. 50675198) and Zhejiang Provincial Natural Science Foundation of China (No. R1090453).

Fangfang Liu and Prof. Can-Jun Yang are with the Institute of Mechatronic and Control Engineering, State Key Lab. of Fluid Power Transmission and Control, Zhejiang University, 310027 P. R. China (phone: 86-571-87953759; e-mail: fangfliu.zju@gmail.com, ycj@zju.edu.cn).

Prof. Kok-Meng Lee is with the George W. Woodruff School of Mechanical Engineering, Georgia Institute of Technology, Atlanta, GA 30332-0405, USA(e-mail: kokmeng.lee@me.gatech.edu), and visiting Pao Yu-Kong Chair Professor at the Zhejiang University.

aquatic propulsion is similar to that used in nature by stingrays, knifefish or cuttlefish. In comparison with traditional methods of propulsion (such as jets and axial propellers), wave-like propulsion systems offer several advantages including low underwater acoustic noise, great maneuverability and better propulsion efficiency at low speeds [6]. Due to these advantages, biomimetic wave-like locomotion systems have significant applications in underwater exploration as they can ensure a safe environment by preserving undisturbed surroundings for data acquisition.

Many biologically inspired robots have been recently proposed based on undulating-finned animals [7-11]. While theoretical [12,13], computational [14-16], and experimental [17,18] researches have been conducted to understand hydrodynamic propulsion performances, the latest existing work on robots with undulatory locomotion has been mainly focused on the latter two methods. A simplified computational model of thrust has been introduced in [19]. Using a two-dimensional unsteady computational fluid dynamics (CFD) method, four basic undulating fin patterns were numerically analyzed in [20] for investigating the effect of different pressure distributions on fin surface and thrust produced. Shirgaonkar and coworkers investigated the hydrodynamics of ribbon-fin propulsion using numerical computation, digital particle image velocimetry (DPIV) measurements and drag measurements [21]. Their results are useful for engineering bio-inspired vehicles with undulatory thrusters.

This paper has been motivated by the need to develop computational models for analyzing the hydrodynamic performance of an undulating fin, which is essential for designing a robotic fish. The remainder of this paper offers the following:

--A robotic fish for experimental investigation and for validating computational hydrodynamic models of an undulating fin has been developed.

--A relatively complete computational model describing the hydrodynamics of an undulating fin is given. Physical values of the geometric and kinematic parameters used in the computation are based on a prototype flexible-fin mechanism so that numerical solutions can be validated experimentally.

--The pressure and velocity distributions acting on the undulating fin have been numerically solved using the finite volume method (FVM), which provides the basis to compute the forces acting on the undulating fin.

--The computational model has been experimentally validated by comparing the computed thrust coefficient

against measured data.

II. OVERVIEW OF THE ROBOTIC FISH SYSTEM

Figure 1(a) shows the CAD model of the radio-controlled robotic fish consisting of three functional units; a mechanical fin, a swing tail, and a gravity allocation module. The oscillating mechanical fin, which propels the fish forward or backward, is driven by a pair of DC-motor actuated crank-slider mechanisms (located at the head and the tail) as shown in Fig. 1(b). The swing tail controls the left/right turning movement of the fish with a servomotor. The relative depth of the fish is weight-regulated by appropriately positioning the worm/gear mechanism in the gravity allocation module.

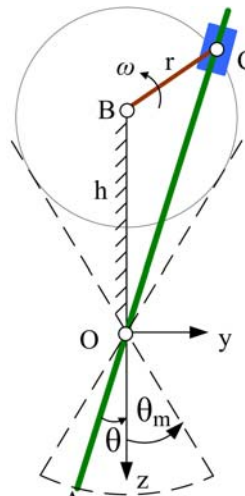
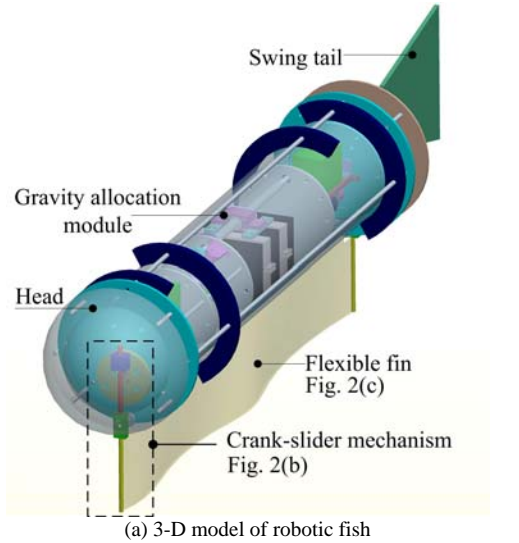
Figure 1(b) schematically shows the motion plane (perpendicular to the motor shaft at point B) of the crank-slider mechanism. As the crank (with radius r) rotates, the link OA (where the flexible fin is affixed) oscillates cyclically within an angular range $\pm\theta_m$ about the point O. In Fig. 1(b) where OB (with length h) is fixed, the vector sum $\mathbf{OB} + \mathbf{BC} = \mathbf{OC}$; hence, the angular displacement of the link OA is given by (1):

$$\theta = \begin{cases} \vartheta & \vartheta \geq 0 \\ \vartheta + \pi & \vartheta < 0 \end{cases} \text{ where } \vartheta = \tan^{-1} \frac{r \sin(\omega t)}{h + r \cos(\omega t)} \quad (1a,b)$$

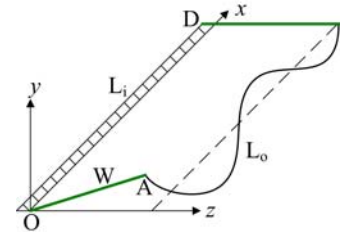
As shown in Fig. 1(c), the inner side OD of the flexible fin is fixed to the fish body. For clarity, the reference coordinate frame (origin O) is defined in Figs. 1(b) and 1(c), where the x-axis is along the fixed edge of the flexible fin while z-axis pointing downward along OB.

By actuating the head crank-slider with respect to its tail mechanism to synchronously undulate the fin, a traveling wave can be generated passing from the head to tail producing the thrust that moves the fish forward. Similarly, the robotic fish can be made to swim backward when the tail crank-slider is actuated with respect to its head mechanism. The generated sinusoidal waveform (with decaying amplitude along the X direction) is not arbitrary but depends significantly on several factors; among these are the fin aspect ratios. For a given mechanism and fin material, different lengths of outer edges are able to generate different wave amplitudes (or number of waves).

To gain intuitive insights and establish a rational basis for investigating the effects of the fin design on the mechanical fish propulsion, the flow fields around the fin and its changes during fin undulation are numerically analyzed. Without loss of generality, we consider only the case where only the head crank-slider is actuated (and the tail end is fixed but parallel to OB) for the three dimensional (3D) unsteady CFD numerical analysis of the flexible fin.



(b) Crank-slider mechanism



(c) Flexible fin
Fig.1 The schematic diagram of robotic fish

III. FORMULATION OF THE CFD ANALYSIS

The unsteady flow field (of the incompressible fluid) around the fin is governed by the Navier-Stokes momentum equations and the equation of continuity in (2a, b):

$$\rho \frac{D\mathbf{V}}{Dt} = \mathbf{F} - \nabla p + \mu \nabla^2 \mathbf{V} \text{ and } \nabla \cdot \mathbf{V} = 0 \quad (2a, b)$$

where ρ and μ are the density and dynamic viscosity of the fluid; \mathbf{V} is the fluid velocity vector; D/Dt is the total time-derivative; \mathbf{F} is the body force acting on the fluid (primarily due to gravity); and p is the pressure.

A. Assumptions

Figure 2 shows the FVM model (for simulating the fluid flow pass the flexible fin within an open-ended rectangular channel with no-slip walls), where

$$x \in [-x_i, x_o], y \in [-y_w, y_w], z \in [-z_l, z_r]$$

where $x_i, x_o, y_w, z_l, z_r > 0$. The momentum equations are spatially discretized with a 1st order upwind scheme while an implicit 1st order scheme is used for temporal discretization

(with time step-size of 0.5ms). The pressure/velocity coupling is handled through the continuity equation using the semi-implicit method for pressure-linked equation (SIMPLE algorithm), valid for small time steps used in the simulation.

For solving the flow field using FVM, the following assumptions are made:

1. The inflow passing through the upstream boundary surface S_i ($x = x_i, y = [-y_w, y_w], z = [-z_l, z_r]$) is steady and uniform.
2. The downstream boundary surface S_o ($x = x_o, y = [-y_w, y_w], z = [-z_l, z_r]$) is far from the flexible fin. The outflow is steady, uniform and equal to the inflow since the fluid is incompressible.
3. The four side-boundary surfaces (S_1, S_2, S_3, S_4) are also far from the flexible fin such that the walls have little or no effects on the flow field around the flexible fin.

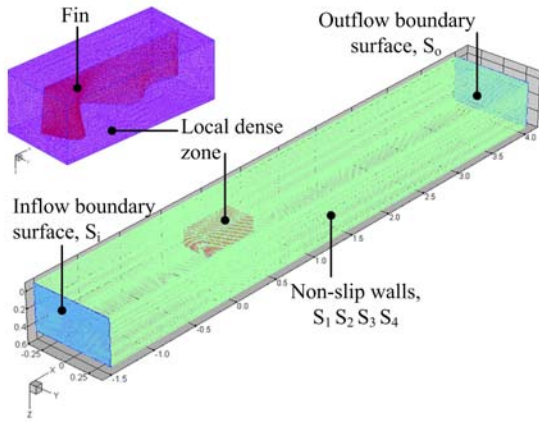


Fig. 2 FVM Model of the flow field

B. Boundary /Initial Conditions

Based on the above assumptions, the boundary conditions essential to solve (2a, b) for a solution that is physically relevant and initial conditions are specified in (3a,b) and (3c):

$$\text{At } S_i \text{ and } S_o, \quad V_x = U, \quad V_y = V_z = 0 \quad (3a)$$

$$\text{At } S_1, S_2, S_3, S_4, \quad \mathbf{V} = 0 \quad (3b)$$

$$\text{At } t = 0 \quad \nabla p = 0, \text{ and } \mathbf{V} = 0 \quad (3c)$$

C. Input Parameters

To simulate the flow field around the flexible fin, the mechanical motion of the flexible fin are specified as an input for a given design geometry. Previous experiments [22] suggest that the undulating fin motion (Fig. 2) has the following form:

$$y(x, z, t) = A(x, z) \sin[2\pi(x/\lambda - ft)] \quad (4)$$

$$\text{where } A(x, z) = az(x + b) \quad (4a)$$

In (4), $A(x, z)$ depicts the wave amplitude; λ and $T=1/f$ are its corresponding wavelength and period respectively; (a, b) are constants to be experimentally determined.

D. Force Models

Once the pressure and velocity distributions are known, the hydrodynamic force acting on the fin surface (and hence the thrust of the robotic fish) due to the undulation motion can be

calculated using the force models discussed with the aid of Fig. 3, which shows the forces (thrust and drag in the horizontal direction, and weight, buoyancy and hydrodynamic lift in the vertical direction) acting on the robotic fish. The hydrodynamic stability and direction of the movement are often considered in terms of roll, yaw and pitch. For understanding the sensitivity of fin design on propulsions, we consider here only the translational motion of the fish (mass m):

$$m \frac{d\mathbf{V}_f(t)}{dt} = \mathbf{F}_T(t) - \mathbf{F}_D(t) \quad (5)$$

where \mathbf{V}_f is the instantaneous velocity of the fish; and \mathbf{F}_T and \mathbf{F}_D are the corresponding thrust and drag acting on the fish. For fishes typically swimming in the range of $10^3 < Re < 5 \times 10^6$, the inertial forces dominate and viscous forces are neglected implying that the force acting on the propulsive element (Fig. 3b) is largely normal to its surface. Thus, the steady-state forces in the x direction at, $F_T(t) = F_D(t)$, can be found from (6a, b):

$$F_T(t) = \int_S p(t) (\mathbf{n}_x \cdot dS) \quad (6a)$$

$$F_D(t) = \frac{1}{2} \rho C_D \int_S [\mathbf{v}(t) \cdot \mathbf{n}_x]^2 dS \quad (6b)$$

where $\mathbf{v}(t)$ is the propulsive element velocity relative to the fluid; and \mathbf{n}_x is the unit vector in the x direction; S is the wetted surface area of the fin; and C_D is the drag coefficient. In (6a), the stress vector $p(t)$ acting on the propulsive element is normal to the surface of the element.

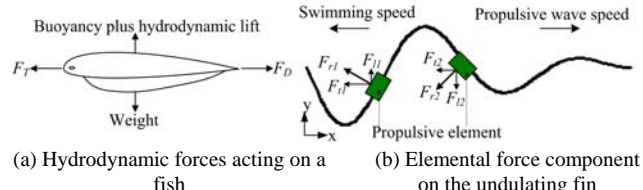


Fig. 3 Schematics illustrating the forces acting on a fish, adapted from [6]

IV. EXPERIMENTAL SETUP AND SIMULATION PARAMETERS

The values of the following parameters are determined experimentally for the FVM simulation of the flow field:

1. The parameters characterizing the wave motion of the fin in (4); specifically, a, b, λ for a given f .
2. The velocity U of the steady uniform inflow in the boundary condition (3a).
3. The thrust F_T for validating the FVM results.

The experiments are performed on the robotic fish developed at the Zhejiang University [22]. The flexible fin is a 0.2mm-thick latex sheet with a trapezoidal shape ($L_i=0.5\text{m}$, $L_o/L_i=1.36$, and $W=0.15\text{m}$). The Reynolds number ($Re=UL_i/v$ where v is kinematic viscosity of the fluid) is in the range at $10^5 \sim 10^6$; the flow is typically turbulence.

A. Parameters in the wave equation (4) of the fin motion

The experimental setup is shown in Fig. 4, where the body of the robotic fish is placed on the top of the rectangular aquarium (0.80m in length, 0.35m in width and 0.30m in

height); and the fin is completely immersed in water below. Illuminated each side of the aquarium with a 1kW lamp, a Canon A620 camera is located below the aquarium filming the projected motion of the undulating flexible fin on the xy-plane (at a rate of 30 frames per second). A typical snap shot is shown in Fig. 5. As a reference, square grids of 2cm are graphed at the bottom of the aquarium to facilitate deriving the enveloping amplitude $A(x, z)$ that characterizes the wave equation (4) from the film. Parameters characterizing the fin and its (experimentally found) motion amplitude are summarized in Table 1.

TABLE 1 FIN AND WAVEFORM PARAMETERS

Description	Parameter	Values
Fin length, m	L_i, L_o	0.5, 0.68
Fin width, m	W	0.15
Latex sheet, mm	thickness	0.2
Experimentally obtained $A(x, z)$:		
Propulsion frequency, Hz	f	4
Propulsion wavelength, m	λ	0.25
Envelop amplitude	(a, b)	(0.2, -0.5)

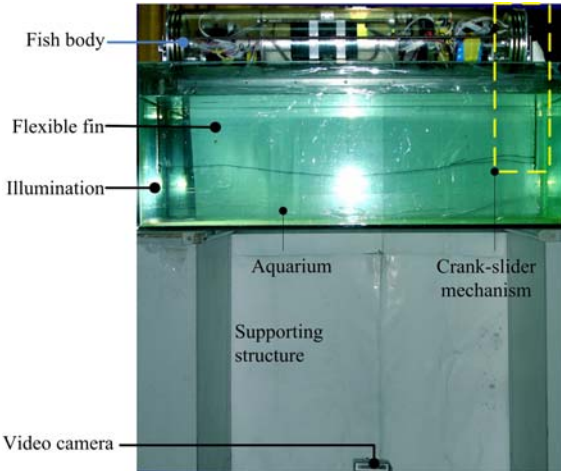


Fig. 4 Experimental setup

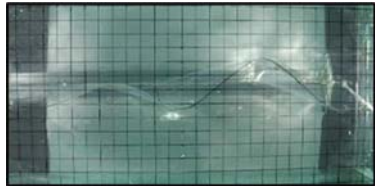
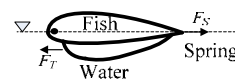


Fig. 5 Typical snap shot characterizing the motion of the undulating fin

Table 2: Experimental data

f (Hz)	4
U (m/s)	0.25
F_T (N)	2.26
C_T	0.97



B. The average velocity U and thrust F_T

To realistically simulate the performance of the flexible fin propulsion, experiments were conducted in a large pool (20m×20m×1m) to determine the average propelling velocity U and force F_T in terms of undulation frequency. As shown in Fig. 1, the robotic fish has a gravity allocation module (designed to balance the body-weight against buoyancy) consisting of a worm/gar mechanism through which the fish centroid can be appropriately adjusted. As schematically illustrated in Table 2, the calibrated scale (with a low spring constant) measures the thrust F_T at a given frequency by

statically balancing it against the spring force F_S . The results are summarized in Table 2, where the thrust coefficient C_T was calculated from (7):

$$C_T = 2F_T / (\rho SU^2) \quad (7)$$

C. Flow visualization

To qualitatively characterize the fin undulation propulsion for intuitively understanding the changes of the fluid velocity during undulation of the robotic fish, a flow visualization experiment is done in a rectangular pool with dimension of 3.5m(L)×2.5m(W)×1.5m(H). In this experiment, the robotic fish floated with the mechanical fin completely submerged in water where small white particles were initially suspended. Motion videos of the small white particles were captured using an underwater video camera as the robotic fish propelled to swim forward. As shown in the sequential snap-shot images in Fig. 6 derived from a camera underwater, particles move backward and downward demonstrating that both thrust and lift are produced during the undulation of the robotic fish, and the force due to the lift is smaller than that due to the thrust.

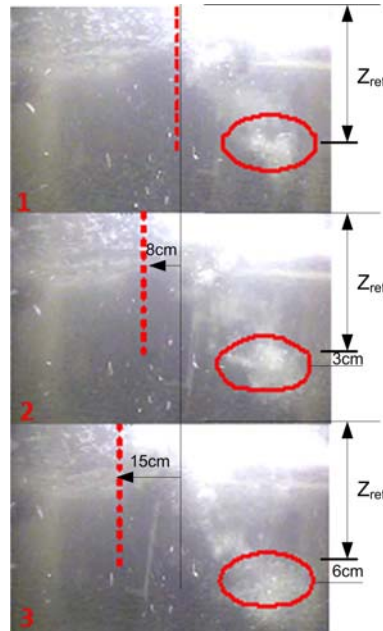


Fig. 6 Particle movements during undulation ($Z_{ref}=38\text{cm}$)

V. RESULTS AND DISCUSSION

To solve the 3D unsteady fluid-flow equations (2a, b) for the velocity V and pressure p around the fin for a specified propulsion frequency f , the finite volume method with an implicit segregated solver approach has been employed. The computational model of (2) with boundary and initial conditions (3) is solved using FLUENT, a commercial finite volume method (FVM) package with a user defined function (written and compiled in Visual C++) linked to the computational fin model to define its motion. The dynamic mesh method is then used in the computation.

The dimension of the computational region is $12L_i$ in

length, $6W$ in width, $6W$ in height, where L_i and W are defined in Fig. 1. The computational mesh consists of 952,378 closer tetrahedral elements around the fin, and the remainder of the domain consists of sparse hexahedral elements. For reducing the computational time while not affecting the accuracy, the dynamic meshes are only updated in the vicinity of the undulating fin, which is referred to here as the local dense zone in Fig. 2. A static mesh is used for the remaining domain. The FVM simulations have been based on experimentally obtained velocity values summarized in Table 2.

Results are presented in Figs. 7 to 9. Fig. 7 are four sequential snap-shots (captured at $t/T= 0.25, 0.5, 0.75$ and 1) during an undulation cycle (period $T=0.25\text{s}$) showing the pressure distribution at $z=0.15\text{m}$. The corresponding velocity distributions around the fin are given in Fig. 8. Figure 9 graphs the thrust coefficient C_T calculated from (7), where the negative sign indicates that the thrust is in the opposite direction of positive x . Observations from these results are discussed:

1. As the actuating link of the fin oscillates about the z -axis (Fig. 1), the pressure and velocity distributions (Figs. 7 and 8) at $t/T= 0.75$ and 1 are mirror images of those at $t/T= 0.25$ and 0.5 as expected. The thrust coefficient C_T (Fig. 9) changes periodically undergoing 2 cycles within the same undulation cycle; C_T has a period of $T/2$. The maximum $|C_T|$ values occur at $t/T=0.5n$ where n is an arbitrary natural number. These instants correspond to the largest velocity of the link OA (Fig. 1) within a cycle, and are consistent with the large relative velocity of the enveloped fluid as observed in Fig. 8.
2. As shown in Fig. 7, regions of positive and negative pressure develop during the fin undulation, which generate a wave transmitting along the $+x$ direction. As a result, the fin reacts to the positive fluid pressure around the fin in the $-x$ direction. Some negative pressure regions can be seen near the wave crests and troughs due to the change in the direction of the fin movement. Large pressure differences generated across the fin are primarily near the actuating end, and decrease along x because wave attenuates and loses energy.

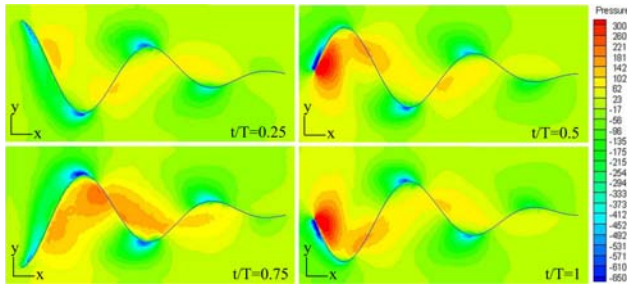


Fig. 7 Pressure Distribution in Pa; $f=4\text{Hz}$, $z=0.15\text{m}$

3. Figure 8(a) shows that the fluid enveloped by the fin has a larger velocity than that away from the fin where the velocity approaches U (the steady uniform inflow velocity), especially in the x direction. Apparently, the reaction of the

undulating fin increases the fluid momentum enveloped by the fin, which can be described by(8):

$$\frac{d}{dt}(m_w \mathbf{V}) \approx \mathbf{F}_w \quad (8)$$

where m_w is the mass of fluid enveloped by the fin; and \mathbf{F}_w is the reaction acting on the fluid. Around the wave crest and trough, the x -component velocity of the fluid not enveloped by the fin is nearly zero or negative corresponding with the pressure distribution.

4. As the fin undulation is symmetrical about the y -axis but asymmetrical about the z -axis, it has different influences on the instantaneous y - and z -component of the fluid velocity as compared between Figs. 8(b) and 8(c). The asymmetrical undulation about the z -axis generates a hydrodynamic lift, while the x -component velocity propels the robotic fish forward. This confirms the results observed in the flow visualization experiment in Fig. 6.

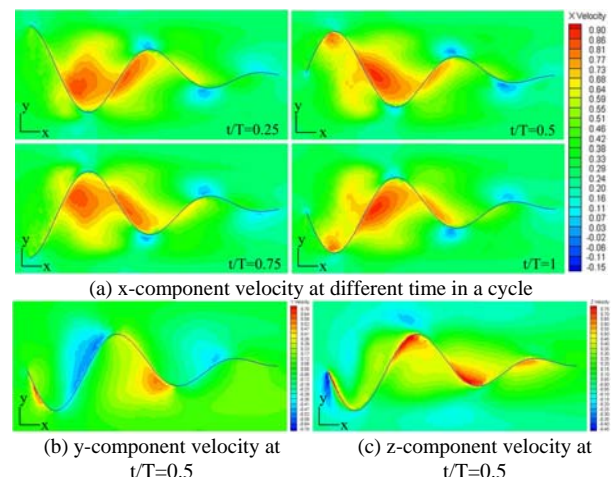


Fig. 8 Distributions of component velocities at $f=4\text{Hz}$ and $z=0.15\text{m}$

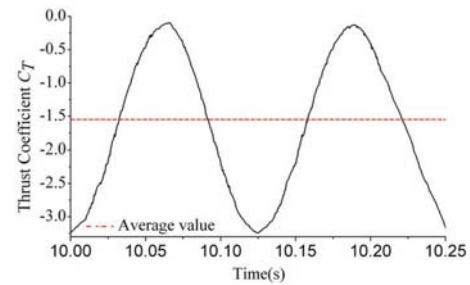


Fig. 9 Thrust coefficient C_T as function of time; $f=4\text{Hz}$

5. The average thrust coefficient at $f=4\text{Hz}$ is $\bar{C}_T = -1.53$. The discrepancy against the experimental result of 0.97 (Table 2) can be accountable to two possible sources. The first could be due to the neglected elastic deformation of the flexible fin under the surrounding fluid pressure; however, estimations based on captured images suggest that elastic deformation has little or no contribution to this discrepancy. Another possible source is the error in the experimental approximation of the fin undulation in the CFD simulation. While the displacements of the undulating fin can be closely characterized from the motion images (Figs. 4 and 5), the actual velocity of the fin undulation was found to be lower

than the idealized sine-function given by (4) used in the CFD simulation. As an illustration, the angular velocity of OA actuated by the crank-slider mechanism is derived from the time-derivative of (1b):

$$\frac{d\theta}{dt} = \omega \frac{\gamma \cos(\omega t) + 1}{\gamma^2 + 2\gamma \cos(\omega t) + 1} \text{ where } \gamma = \frac{h}{r}. \quad (9)$$

Fig. 10 compares the speed derived from (4) using the values experimentally obtained from images (Fig. 5) as inputs for the FVM against the actual link speed at tip A (Fig. 1) during the fin undulation. Since the drag force F_D is proportional to the square of the velocity, the over-estimated thrust coefficient in the simulation is consistent with the experimental data obtained using the actual robotic fish. From (9),

$$d\theta/dt \rightarrow \omega/2 \text{ as } \gamma = h/r \rightarrow 1.$$

The above implies that (4) closely approximates the actual displacement and velocity at the tip A of the link OA when the crank-slider mechanism is designed such that $h \rightarrow r$.

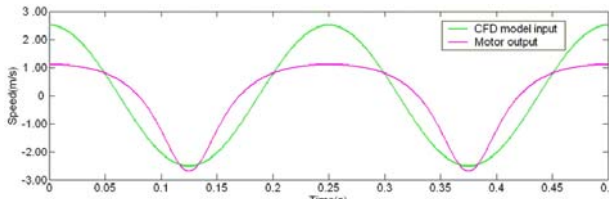


Fig. 10 Comparison between the actual link speed at tip A (Fig. 1) and speed derived from equation (4) for FVM simulation; $f=4\text{Hz}$

VI. CONCLUSION & FUTURE WORK

A fin-based robotic fish along with its hydrodynamic model has been presented. Underwater experiments were performed for flow visualization and for determining physical values of key parameters used in the numerical analysis; along with a relatively complete computational model, the findings provide the rationale basis for investigating the effect of fluid flow field around the mechanical fin on propulsion performance. The results confirm that asymmetrical undulation about the z -axis generates a hydrodynamic lift while the x -component velocity propels the robotic fish forward. This asymmetrical hydrodynamic lift, however, can be eliminated in a dual-fin design employing a pair of symmetric fins commonly seen in natural fin-based fish such as stingray, knife fish and cuttlefish. The discrepancy against the experimental result is due to the fin-undulation approximation used as input in the CFD simulation, where the actual velocity of the fin undulation is lower than the sine-function assumed in the CFD simulation.

ACKNOWLEDGMENT

The authors thank Mr. Jing-hui Zheng for technical helps in developing the robotic fish.

REFERENCES

- [1] J.E. Colgate, K.M. Lynch, "Mechanics and control of swimming: a review," IEEE Trans. of Ocean. Eng., vol. 29, no. 3, pp. 660-673, 2004.
- [2] S. Guo, T. Fukuda, and K. Asaka, "A new type of fish-like underwater microrobot," IEEE/ASME Trans. on Mechatronics, V. 8, no. 1, pp. 136–141, 2003.
- [3] H. Hu, J. Liu, I. Dukes, and G. Francis, "Design of 3D swim patterns for autonomous robotic fish," in Proc. 2006 IEEE/RSJ Int. Conf. Intell. Robots Syst., Beijing, China, pp. 2406–2411, 2006.
- [4] G. V. Lauder, E. J. Anderson, J. Tangorra, P. G. A. Madden, "Fish biorobotics: kinematics and hydrodynamics of self-propulsion," The Journal of Experimental Biology, vol. 210, pp. 2767-2780, 2007.
- [5] V.V. Krylov, G.V. Pritchard, "Experimental confirmation of the propulsion of marine vessels employing guided flexural waves in attached elastic fins," J. Fluid. Struct., vol. 23, pp. 297-307, 2007.
- [6] Sfakiotakis, M., Lane, D.M., Davies, J.B.C., "Review of fish swimming modes for aquatic locomotion," IEEE J. of Ocean. Eng., vol. 24, pp. 237-252, 1999.
- [7] Low, K.H., Willy, A., "Development and initial investigation of NTU robot fish with modular flexible fins," in Proc. IEEE Int. Conf. Mechatronics & Automation, Niagara Falls, Canada, 2005.
- [8] M. Epstein, J.E. Colgate, M.A. MacIver, "A biologically inspired robotic ribbon fin," in Proc. IEEE/RSJ Int. Conf. Intelligent Robots and Systems, Edmonton, Alberta, Canada, 2005.
- [9] M. Yamamura, K. Takagi, Z. Luo, et al, "An autonomous ray-like swimming robot with IPMC artificial muscle," Proceedings of the Third Conference on Artificial Muscles - A Nanobiotechnology Research: The Perspective of artificial Muscles , May 2006.
- [10] Y. Zhang, J.H. He, J. Yang, S.W. Zhang, K.H. Low, "Design and investigation of shape memory alloy driven flexible pectoral fin," in Proc. IEEE Int. Conf. Robotics and Biomimetics, Kunming, China, 2006.
- [11] T. Hu, L. Shen, L. Lin, et al, "Biological inspirations, kinematics modeling, mechanism design and experiments on an undulating robotic fin inspired by *Gymnarchus niloticus*," Mechanism and Machine Theory, vol. 44, pp. 633-645, 2009.
- [12] M. J. Lighthill, "Large-amplitude elongated-body theory of fish locomotion," in Proc. R. Soc. Lond. B, 1971, vol. 179, pp. 125–138.
- [13] T. Y. Wu, "Mathematical biofluid dynamics and mechanophysiology of fish locomotion," Math. Methods Appl. Sci., vol. 24, pp. 1541–1564, 2001.
- [14] R. Mittal, "Computational modeling in biohydrodynamics: Trends, challenges, and recent advances," IEEE J. Ocean. Eng., vol. 29, no. 3, pp.595–604, Jul. 2004.
- [15] H. Suzuki and N. Kato, "A numerical study on unsteady flow around a mechanical pectoral fin," International Journal of Offshore and Polar Engineering, Vol. 15(3), pp. 161–167, 2005.
- [16] K. Abdelnour, E. Mancia, S. D. Peterson, et al, "Hydrodynamics of underwater propulsors based on ionic polymer metal composites: A numerical study," Smart Mater. Struct., vol. 18(8), pp. 1-11, 2009.
- [17] J. Peng, J. O. Dabiri, P. G. Madden, and G. V. Lauder, "Non-invasive measurement of instantaneous forces during aquatic locomotion: A case study of the bluegill sunfish pectoral fin," J. Exp. Biol., vol. 210, pp. 685–698, 2007.
- [18] S. D. Peterson, M. Porfiri, A. Rovardi, "A particle image velocimetry study of vibrating Ionic Polymer Metal Composites in aqueous Environments," IEEE/ASME Trans. on Mechatronics, vol. 14(4), pp. 474-483, 2009.
- [19] M. Epstein, J. E. Colgate, and M. A. MacIver, "A Biologically Inspired Robotic Ribbon Fin," presented at IEEE/RSJ International Conference on Intelligent Robots and Systems, Edmonton, Alberta, Canada, 2005.
- [20] Y. Zhang, L. B. Jia, S.W. Zhang, Yang, J., K.H. Low, "Computational research on modular undulating fin for biorobotic underwater propulsor," J. Bio. Eng., vol. 4, pp. 25-32, 2007.
- [21] A. S. Anup, M. C. Oscar, A. P. Neelesh, et al, "The hydrodynamics of ribbon-fin propulsion during impulsive motion," The Journal of Experimental Biology, vol. 211, pp. 3490-3503, 2008.
- [22] F. F., Liu, C. J. Yang, Y. Q. Xie, et al, "Initial development and experiments on a robotic fish with a novel undulating fin," in Proc. 2008 IEEE Conf. on Robotics, Automation and Mechatronics, Chengdu, China, pp. 1075-1078, 2008.